ELSEVIER

Journal of Molecular Catalysis A: Chemical 141 (1999) 223–240

JOURNAL OF MOLECULAR CATALYSIS A: CHEMICAL

Templating fabrication of platinum nanoparticles and nanowires using the confined mesoporous channels of FSM-16—their structural characterization and catalytic performances in water gas shift reaction

Makoto Sasaki, Mai Osada, Naonori Higashimoto, Takashi Yamamoto, Atsushi Fukuoka, Masaru Ichikawa *

Catalysis Research Center, Hokkaido University, Sapporo, 060 Japan

Abstract

The robust trigonal prismatic Pt_{18} and Pt_{15} cluster anions are selectively synthesized via $[Pt(CO)Cl_3]^-$ in FSM-16 (4.7 nm) and *cis*-$Pt(CO)_2Cl_2$ in FSM-16 (2.8 nm) by the reductive carbonylation of H_2PtCl_6 in the confined mesoporous channels of FSM-16, respectively. The Pt cluster anions extracted from the resulting samples in the THF solution by cation metathesis with [PPN]Cl are identified as $[Pt_3(CO)_6]_5^{2-}$ in FSM-16 (2.8 nm) and $[Pt_3(CO)_6]_6^{2-}$ in FSM-16 (4.7 nm) by the FTIR and UV–Vis spectroscopic data. The EXAFS and FTIR studies demonstrated that $[Pt_3(CO)_6]_5^{2-}$/FSM-16 (2.8 nm) ($\nu_{CO} = 2078$, 1880 cm^{-1}) and $[Pt_3(CO)_6]_6^{2-}$/FSM-16 (4.7 nm) ($\nu_{CO} = 2056$, 1879 cm^{-1}) were transformed by heating at 300–343 K into the partially decarbonylated Pt clusters (Pt–Pt; C.N. = 7.6, $R = 2.73$ Å) characteristic of a linear CO band ($\nu_{CO} = 2015$ cm^{-1}). According to the EXAFS and TEM observation, Pt carbonyl clusters are eventually converted above 473 K to naked Pt particles of 11 Å (Pt–Pt C.N. = 6.7, $R = 2.72$ Å) in FSM-16 (2.8 nm) and of 15 Å (C.N. = 7.9, $R = 2.74$ Å) in FSM-16 (4.7 nm). On the other hand, the platinum nanowires [2 and 4 nm (diameter) × 50–500 nm (long)] are prepared using the cylindrical mesoporous channels of FSM-16 (2.8 and 4.7 nm) in the templating reduction of H_2PtCl_6 by the exposure to γ-ray or UV-light ($\lambda_{max} > 254$ nm) under the atmosphere of 2-propanol and water. It was demonstrated by the TEM observation and EXAFS characterization that the diameters of Pt nanowires formed in FSM-16 are consistent with those of FSM-16 used (2.8 and 4.7 nm), whereas the average lengths of Pt wires are varied by the function of the Pt loading mass and time exposure to γ-ray and UV-light. The observed electron beam diffraction patterns indicate that the Pt wires consist of a single crystal phase of Pt(110) having a lattice fringe of 2.27 Å. It is of interest to find that the Pt nanowires in FSM-16 (2.8 nm and 4.7 nm) exhibited an unique IR spectrum in CO chemisorption and the remarkable activities per surface Pt atom (TOF) for water gas-shift reaction at 323–393 K by 60–90 times larger than those of Pt nanoparticles in FSM-16 and even conventional metal catalysts.

Keywords: Pt cluster anions; Pt nanoparticle; Pt nanowires; Templating synthesis; Mesoporous FSM-16; FTIR/EXAFS/TEM characterization; WGSR

* Corresponding author. Tel.: +81-11-706-2912; Fax: +81-11-706-4957; E-mail: michi@cat.hokudai.ac.jp

1381-1169/99/$ - see front matter
PII: S1381-1169(98)00266-0

1. Introduction

Nanostructured metal/alloy particles and wires in the micro/mesoporous space have attracted growing interests both in their 'confined assembling catalysis' and 'quantum size effects'. Such nanostructured materials are potential for tailor-made metal catalysts [1], electronics, non-linear optics and magnetic devices [2–4]. Zeolites are aluminosilicate crystallites consisting of microporous cavities and channels of molecular dimensions (6–13 Å) with smaller windows. Such micropores can supply 'a templating circumstance' for the selective synthesis of some bulky metal carbonyl clusters which fit to the interior cages as a 'nanometer-size reaction vessel'. We have recently developed [5–8] the concept of 'ship-in-bottle' technique for a templating synthesis of uni- and bimetal carbonyl clusters such as $Rh_{6-x}Ir_x(CO)_{16}$ ($x = 0$–6) [9–11], $HRu_6(CO)_{18}^-$ [12] and $[Pt_3(CO)_6]_n^{2-}$ ($n = 3,4$) [13–17] which are encapsulated in the NaY micropores of 1.3 nm. They exhibit the higher catalytic stabilities and activities for alkane hydrogenolysis [10,11], CO hydrogenation towards C_1–C_5 alcohols [18–21] and methane homologation to lower hydrocarbons [22] in comparison with the conventional metal catalysts.

Recently, mesoporous molecular sieves such as MCM-41 [23,24] and FSM-16 [25,26] have been synthesized using different micelle surfactant templates. These materials are consisting of the ordered mesoporous channels of 2–10 nm diameter, which are much larger than those of the conventional zeolites such as ZSM-5, AlPO-5, and NaY. They are potential hosts for including bulky organometallic complexes [27] and metal particles which are accessible to larger substrates in the catalytic reactions. Additionally, they have been used for the templating fabrication of the quantum dots and wires of metals [8,28] and chalcogenides [2–4].

Chini-type Pt carbonyl clusters such as $[Pt_3(CO)_6]_n^{2-}$ ($n = 2$–10) are synthesized by the reductive carbonylation of Pt salts such as H_2PtCl_6 and $Pt(CO)Cl_3$ in solution [29,30]. Chang et al. [31] have previously reported a surface-mediated synthesis of the Chini-complexes by the reaction of H_2PtCl_6 on MgO and silica. Furthermore, we have demonstrated that a three-stacked $[Pt_3(CO)_6]_3^{2-}$ and four-stacked $[Pt_3(CO)_6]_4^{2-}$ are synthesized in the micropores of NaY (1.3 nm) by the reductive carbonylation of $[Pt(NH_3)_4]^{2+}$/NaY and Pt^{2+}/NaY [14,15], respectively. However, owing to the size limitation of the zeolite micropores, so far more than five-stacked clusters ($[Pt_3(CO)_6]_n^{2-}$ have not been synthesized in NaY and mordenite by a ship-in-bottle technique. We reported preliminarily that a five-stacked $[Pt_3(CO)_6]_5^{2-}$ is uniformly synthesised in the mesoporous channels of FSM-16 by a similar carbonylation of H_2PtCl_6 with CO and H_2O [32,33]. The present work was initiated to extend the intrazeolitic synthesis of larger Pt carbonyl clusters such as $[Pt_3(CO)_6]_n^{2-}$ ($n > 5$), using a mesoporous host of FSM-16 having the larger channels of 2.8 and 4.7 nm. The confined Pt carbonyl cluster anions formed in FSM-16(2.8 and 4.7 nm) were characterized by FTIR, UV–Vis, and EXAFS spectroscopy. The successive transformation of the Pt cluster anions in FSM-16 towards the Pt particles of nanometer size has also been studied by EXAFS and FTIR spectroscopy, coupled with the TEM observation. On the other hand, the reduction of H_2PtCl_6 in FSM-16 (2.8 and 4.7 nm) with 2-propanol and water has been studied by the exposure to γ-ray or UV-light ($\lambda_{max} > 254$ nm) at 300 K. The cylindrical Pt wires of nanometer size in the mesoporous channels of FSM-16 have been characterized by TEM and EXAFS studies including the chemisorption of CO and H_2. This paper reports turnover rates for the water gas shift reaction ($CO + H_2O = CO_2 + H_2$) at 300–393 K on the supported catalysts of Pt nanowires and Pt nanoparticles in FSM-16 (2.8 and 4.7 nm), compared with those of $[Pt_3(CO)_6]_n^{2-}$ ($n = 3$, 4 and 5) encapsulated in NaY and FSM-16. The catalytic behaviors and gas chemisorption of the Pt nanowires and nanoparticles in FSM-16 are dis-

cussed in conjunction with their anisotropic confinement in the micro/mesoporous space as well as the cluster–support interaction.

2. Experimental and procedures

2.1. Sample preparation

2.1.1. Preparation of mesoporous materials FSM-16

According to the published procedures [25,26], the host FSM-16 having channel sizes of 2.8 and 4.7 nm was synthesized from a commercial-grade Kanemite as a layered aluminosilicate ($SiO_2/Al_2O_3 = 320$, Fe: below 0.02%, supplied by Hokkaido Soda) using $C_{16}H_{33}NMe_3Cl$ and $C_{16}H_{33}NMe_3Cl$/mesitylene as a surfactant template, respectively, similar to MCM-41. After washing with water to remove a residual Na^+, the resulting material of FSM-16 thus prepared using $C_{16}H_{33}NMe_3Cl$ was calcined to remove the organic template under a O_2 flow (25 ml/min) at 823 K for 14 h; the calcined material of FSM-16 (2.8 nm) presents well-defined hexagonal channels characteristic of the X-ray powder patterns in the low angle region ($2\theta = 2.26$, 3.44, 4.50 and 5.90), which were confirmed by the TEM observation. Nitrogen adsorption isotherm (measured by Omnisorp-100CX; Coulter) showed uniform pore size distribution at 2.8 and 4.7 nm and specific surface area of 980–1030 m^2/g.

2.1.2. The reductive carbonylation of H_2PtCl_6 in FSM-16 having the channel size of 2.8 and 4.7 nm

The powdered FSM-16 (2.8 and 4.7 nm) was impregnated with a quartanary alkyl ammonium salt NEt_4Cl from an aqueous solution; this is referred to as NEt_4Cl/FSM-16 (1.37×10^{-4} mol/g_{cat}), H_2PtCl_6 was impregnated with FSM-16 and NEt_4Cl/FSM-16 from an aqueous solution, resulting in the samples of 5.0 mass wt.% Pt H_2PtCl_6/FSM-16 and H_2PtCl_6/NEt_4Cl/FSM-16, respectively.

Each powdered sample was exposed to a mixture of CO (26.7 kPa) and H_2O (2.7 kPa) in a closed circulating reactor for 5–15 h by heating from 300 to 323 K for 5–12 h, resulting in the stoichiometric formation of $[Pt_3(CO)_6]_5^{2-}$ in FSM-16 (2.8 nm) and $[Pt_3(CO)_6]_6^{2-}$ in FSM-16 (4.7 nm), respectively. The Chini-type Pt carbonyl cluster anions were independently synthesised from H_2PtCl_6 in an alkaline solution of methanol, and isolated with tetraethylammonium chloride as $[NEt_4]_2[Pt_3(CO)_6]_n^{2-}$ ($n = 3$, 4 and 5) according to the literature method [30]. The reference samples of $[Pt_3(CO)_6]_3^{2-}$ and $[Pt_3(CO)_6]_4^{2-}$ encapsulated in NaY zeolite were prepared by a similar reductive carbonylation of $[Pt(NH_3)_4]^{2+}$/NaY and Pt^{2+}/NaY, respectively according to 'ship-in-bottle' technique [14,15].

2.1.3. Sample preparation of Pt nanowires in FSM-16 by γ-ray radiolysis and ultra-violet illumination

A sample of H_2PtCl_6/FSM-16 containing 3–10 mass% Pt was prepared by impregnation of FSM-16 slurry with H_2PtCl_6 from an aqueous solution. The dried sample was charged in a quartz-glass cell (15×55 mm, 1.5 mm thick), which was irradiated by γ-ray for 5–24 h at 300 K under the atmosphere of 2-propanol (6.8 kPa) and CO (26.7 kPa)/water (2.7 kPa). The sample cell was exposed to γ-ray (adsorbed dose disintegration of 5000 Ci) in a panoramic reactor at Laboratory using ^{60}Co as a γ-ray source (Radioisotope Center, Faculty of Engineering, Hokkaido University). The powdered sample of H_2PtCl_6/FSM-16 changed the color uniformly from pale yellow to gray, which was indicative of its reduction progress. On the other hand, the sample of 5 mass% Pt H_2PtCl_6/FSM-16 charged in a quartz-cell was exposed at 300 K to the UV-illumination of high-pressure Hg lamp (USHIO; UM-102, $\lambda > 254$ nm) for 2–5 h under the vapor of 2-propanol (25–30 kPa) and water (2 kPa).

2.2. IR and UV–Vis spectroscopy and TEM observation

The impregnated samples such as H_2PtCl_6/FSM-16 (2.8 and 4.7 nm), or H_2PtCl_6/NR_4X/FSM-16 (2.8 and 4.7 nm) were pressed into a self supporting wafer (1.5 mm i.d., 12–20 mg/cm^2) with pressure of 300 kgf/cm^2. The wafer was mounted in an in situ IR cell equipped with CaF_2 windows. IR spectra were recorded using a Fourier Transform Infrared spectrometer (Shimadzu FTIR 8100 M) with the resolution of 2 cm^{-1}, and 100 interferrogram were accumulated to improve signal/noise ratios of IR spectra.

The diffuse reflectance UV–Vis spectra for the powdered sample of Pt carbonyl complexes formed in FSM-16 charged in a quartz-plated cell (1 mm thickness) and the absorption spectra of the extracted species in solution were recorded using Shimadzu UV–Vis spectrometer under the nitrogen and CO atmosphere at 300 K.

Transmission electron micrographs were taken using a JEOL JEM-2000EX at an accelerating voltage of 200 kV, similarly as described elsewhere [32,33]. The powder samples were dispersed on a carbon foil with a microgrid from the suspended solution of ethanol and acetone. The TEM images were observed with a minimum damage to the structures and morphology of the samples by the electron beams.

2.3. EXAFS measurement and analysis

The powdered and disk samples were charged under N_2 in an in situ EXAFS cell with a KAPTON film window (500 μm) to prevent exposure of the sample to air. Pt-L_{III} edge (11562 eV) EXAFS (extended X-ray absorption fine structure) spectra were measured at BL-10B at Photon Factory of National Laboratory for High Energy Physics (KEK-PF; Tsukuba, Japan). The energy and the current of the electron (or positron) were 2.5 GeV and 250 mA, respectively. Si(311) channel cut monochromator was used. The spectra were analyzed by a computer program supplied by Technos [34]. The k^3 weighted EXAFS function was Fourier Transformed into R-space using the k-range from 3.5 to 18 Å^{-1}; The Hanning function used was $\delta = 0.5$ Å^{-1}. The phase shift was not corrected for the preliminary Fourier transformation. The inverse Fourier transform was calculated to obtain a filtered EXAFS function. The R range of an inverse Fourier transformation was taken from 1.09 to 3.31 Å; The Hanning function of $\Delta = 0.05$ Å was used as a window function. The fitting EXAFS parameters of the sample were determined for N_i and r_i, to minimize σ_i and correction of threshold energy (ΔE_0). The backscattering amplitudes and phase shift functions of Pt–Pt, Pt–C and Pt–O (of Pt–CO) bondings are corrected using those of Pt foil (Pt–Pt) and $W(CO)_6$ (Pt–C and Pt–O). The EXAFS parameters for discussion were fixed around the optimum value, and the residual factor R was calculated to offer the optimum values for the other parameters [35].

2.4. Catalytic reactions and CO / H_2 chemisorption

The catalytic reactions were carried out using a closed circulating system equipped with a pyrex-glass tubing reactor, which mounted each sample of 50 mg. The water gas shift reaction was conducted at the temperatures of 278–493 K. Pressures of reactant gases were $p(H_2O)$ = 2.6 kPa; $p(CO)$ = 50–210 kPa. The dead volume of the reactor was 250 cm^3. Products were analyzed by a Shimadzu 8A gas-chromatography (gc) with a TCD (thermal conductive detector) using the columns Molecular Sieve 5A for CO, H_2 and CH_4, and Porapak Q for CO_2 and H_2O (4 m, 313 K), respectively. Helium was used as a carrier gas (30 ml/min) for the gc analysis.

Chemisorption of CO was measured at 300 K in a constant-volume adsorption system. Before the chemisorption experiment, the sample (Pt

nanoparticle/FSM-16 and Pt nanowire/FSM-16) was heated in H_2 at 573 K for 1 h, evacuated at this temperature for 0.5 h to 1×10^{-3} kPa). An initial isotherm was taken to measure total CO uptake. Then the sample was evacuated at 300 K for 0.5 h and the second isotherm was obtained to measure weakly adsorbed CO. The isotherms were extrapolated zero pressure and the difference in CO (or H_2) uptake at that pressure was taken as the amount of the irreversible chemisorption on the samples of Pt nanoparticle/FSM-16 and Pt nanowire/FSM-16.

3. Results and discussion

3.1. Synthesis and characterization of the confined Pt cluster anions in FSM-16 by the reductive carbonylation

The sample of 5.0 mass% Pt H_2PtCl_6/NEt_4Cl/FSM-16 (2.8 and 4.7 nm) were exposed to CO (20.5 kPa) and a mixture of CO (20.5 kPa) and H_2O (2.0 kPa) by heating from 300 to 323 K in a closed circulating system. After the exposure of H_2PtCl_6 in NEt_4Cl/FSM-16 (4.7 nm) to CO the reaction was measured by the in situ IR spectroscopy. The CO band appeared firstly at 2106 cm^{-1} which is assignable to $[Pt(CO)Cl_3]^-$. This CO band was developed by heating the pale yellow sample as shown in Fig. 1a–d. By contrast to this, the sample of H_2PtCl_6/NEt_4Cl/FSM-16 (2.8 nm) yielded the intense twin CO bands at 2188 and 2148 cm^{-1} due to *cis*-$Pt(CO)_2Cl_2$ with a minor contribution of $[Pt(CO)Cl_3]^-$ (2116 cm^{-1}). From the analogy of the reference Pt carbonyl species [36–38], the latter twin CO bands can be assigned to *cis*-$Pt(CO)_2Cl_2$ (2188 and 2148 cm^{-1} in methanol solution). The mono-Pt carbonyl species $[Pt(CO)Cl_3]^-$ in FSM-16 (4.7 nm) was subsequently converted at 323 K by the admission of a mixture of CO and H_2O, leading to the final IR spectrum of the reddish-brown sample consisting of two intense bands

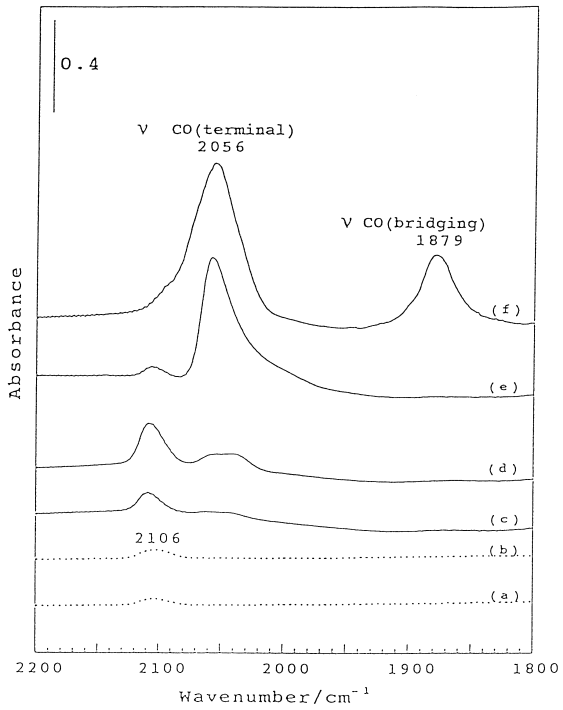

Fig. 1. IR spectra of carbonyl species formed by the reductive carbonylation of H_2PtCl_6/NEt_4Cl/FSM-16 (4.7 nm). The disk sample of H_2PtCl_6/NEt_4Cl/FSM-16 (4.7 nm) was exposed to CO (p(CO) = 26.6 kPa) at 323 K for (a) 1 h and (b) 3 h. Then the sample was exposed to CO + H_2O (p(CO) = 26.6 kPa, p(H_2O = 2.0 kPa) at 323 K for (c) 1 h, (d) 3 h, (e) 12 h, and (f) 24 h. The background IR absorption spectrum of H_2PtCl_6/NEt_4Cl/FSM-16 was subtracted from each spectrum recorded after the admission of CO and a mixture of CO and H_2O to the sample.

of the linear CO at 2056s and bridging CO at 1879m cm^{-1} as shown in Fig. 1e–f. As it was previously reported [31], a dark-green sample was similarly formed via the intermediate of *cis*-$Pt(CO)_2Cl_2$ by the reductive carbonylation of H_2PtCl_6/NEt_4Cl/FSM-16 (2.8 nm) with CO + H_2O at 300–323 K; The resulting solid sample showed two intense IR carbonyl bands at 2086s and 1880m cm^{-1}, which has been identified as $[Pt_3(CO)_6]_6^{2-}$ in FSM-16 (2.8 nm). The CO bands observed in H_2PtCl_6/NEt_4Cl/FSM-16 (2.8 and 4.7 nm) after the prolonged carbonylation reaction with CO and water closely resemble those of the Chini-type Pt carbonyl clusters such as $[Et_4N]_2[Pt_3(CO)_6]_n$ where $n = 3$–5 in solution [29,30] and the sur-

face-grafted Pt cluster anions on SiO_2, Al_2O_3 and MgO [31,39,40] as exemplified in Table 1.

3.2. Extraction of the Pt cluster anions by cation metathesis and IR / UV–Vis characterization

The attempts to extract the Pt carbonyl species from the resulting sample of the Pt carbonyl cluster anions in FSM-16 (2.8 and 4.7 nm) were conducted by the cation metathesis using $[(Ph_3P)_2N]Cl$ (triphenylphosphoranylidene ammonium chloride) in THF (tetrahydrofuran) and MeOH as a polar solvent. Figs. 2 and 3 show the IR and UV–Vis spectra of the Pt carbonyl cluster anions with PPN^+, which were extracted in THF, respectively. In comparison with that of $[NEt_4]_2[Pt_3(CO)_6]_6$ in MeOH [29,30], it was found that the IR spectrum (Fig. 2) of the

Table 1
IR carbonyl bands of different Pt carbonyl complexes having different nuclearity

Pt atom number	Complexes	/Support/pores/solvent	ν CO [cm^{-1}] (linear, bridged)	Reference
1	PtO(CO)	/γ-Al_2O_3	2120	[41]
		/NaY	2100	[14,15]
		/FSM-16 (2.8, 4.7 nm)	2116	This work
	$[Pt(CO)Cl_3]^-$	/HCl	2113	[36–38]
		/FSM-16 (2.8 nm)	2116	[14,15], this work
		/FSM-16 (4.7 nm)	2106	This work
	cis-$Pt(CO)_2Cl_2$	/$SOCl_2$	2179, 2136	[36–38]
		/FSM-16 (2.8 nm)	2188, 2148	[14,15], this work
	trans-$Pt(CO)_2Cl_2$	/$SOCl_2$	2136	[38,42]
3	$[Pt_3(CO)_3(\mu_2-CO)_3]^{2-}$	/THF	1995 1810	[29,30]
		/NaX	2025 1790	[16,17]
		/NaY	2112, 1896, 1841	[14,15]
6	$[Pt_3(CO)_3(\mu_2-CO)_3]_2^{2-}$	/THF	1995, 1810	[29,30]
		/γ-Al_2O_3	1970, 1790	[40]
9	$[Pt_3(CO)_3(\mu_2-CO)_3]_3^{2-}$	/THF	2030,1840	[29,30]
		/γ-Al_2O_3	2005, 1810	[40]
		/NaY	2056, 1798	[14,15]
12	$[Pt_3(CO)_3(\mu_2-CO)_3]_4^{2-}$	/THF	2045, 1860	[29,30]
		/MeOH	2050, 1865	[29,30]
		/γ-Al_2O_3	2025, 1830	[40]
		/MgO	2046, 1846	[31]
		/NaY	2080, 1824	[13–15]
15	$[Pt_3(CO)_3(\mu_2-CO)_3]_5^{2-}$	/THF	2055, 1870	[29,30]
		/MeOH	2056, 1873	This work
		/γ-Al_2O_3	2040, 1850	[43]
		/MgO	2059, 1877, 1853	[31]
		/SiO_2	2065, 1865	[39,40]
		/FSM-16 (2.8 nm)	2085, 1882	[32], this work
		/NEt_4NCl/FSM-16 (2.8 nm)	2075, 1875	[32,33], this work
18	$[Pt_3(CO)_3(\mu_2-CO)_3]_6^{2-}$	/THF	2065, 1875	[29,30]
		/MeOH	2065, 1875	[29,30]
		/FSM-16 (4.7 nm)	2065 1878	This work
		/NEt_4NCl/FSM-16 (4.7 nm)	2056 1879	This work
19	$[Pt_{19}(CO)_{12}(\mu_2-CO)_{10}]^{2-}$	/CH_3CN	2000 1795	[41]
24	$[Pt_{24}(CO)_{22}(\mu_2-CO)_8]^{2-}$	/THF	2040 1815, 1797	[44,45]
		/CH_2Cl_2	2047, 1809, 1798	[44]
26	$[Pt_{26}(CO)_{23}(\mu_2-CO)_9]^{2-}$	/CH_2Cl_2	2048 1803	[44]
38	$[Pt_{38}(CO)_{44}]^{2-}$	/CH_2Cl_2	2058 1805	[44]

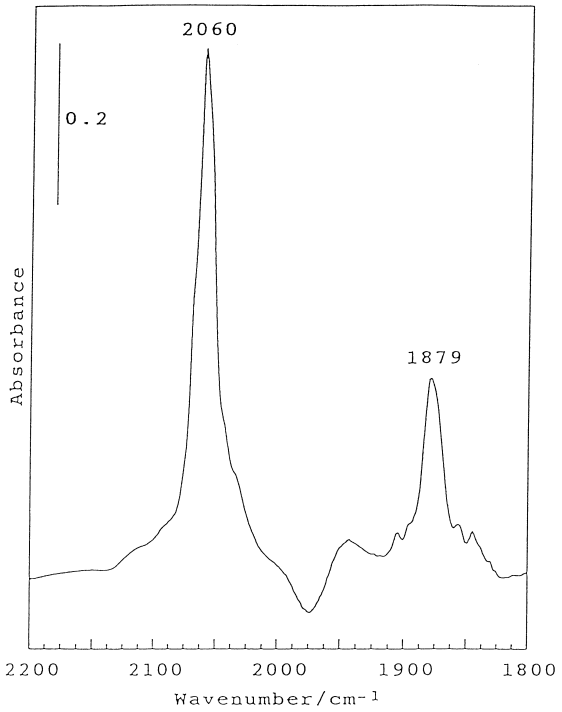

Fig. 2. IR spectra of Pt carbonyl species extracted with [PPN]Cl([$(Ph_3P)_2N$]Cl) in THF from the sample of H_2PtCl_6/NEt_4Cl/FSM-16 (4.7 nm) after the reductive carbonylation at 323 K.

extracted sample (2060vs cm^{-1} for a linear CO and 1879m cm^{-1} for a bridging CO) is in a good agreement with those of a six-stacked $[Pt_3(CO)_6]_6^{2-}$ in MeOH solution (2065vs and 1875m cm^{-1}), only except for a minor shoulder band. The UV–Vis absorption spectrum of the extracted sample in THF (Fig. 3) was observed at 413 and 708 nm, which also resembles that of $[Pt_3(CO)_6]_6^{2-}$ in MeOH ($\lambda_{max} = 410$ and 705 nm) [29,30]. The IR carbonyl bands and UV–Vis spectra of the family of Chini-type complexes $[Pt_3(CO)_6]_n^{2-}$ ($n = 2$–10) in solution depend basically on the size of Pt cluster dianions. Comparing with the characteristic CO bands and UV–Vis spectrum, the Pt cluster anions formed in FSM-16 (4.7 nm) is assigned to $[Pt_3(CO)_6]_6^{2-}$. Accordingly, the IR and UV–Vis data in Figs. 1–3 and Table 1 reasonably reveal that a larger Chini cluster anion $[Pt_3(CO)_6]_6^{2-}$ (8 Å × 15 Å) is encapsulated in a larger channel of FSM-16 (4.7 nm), compared with the confined Pt cluster anions such as $[Pt_3(CO)_6]_5^{2-}$ in FSM-16 (2.8 nm), $[Pt_3(CO)_6]_4^{2-}$ and $[Pt_3(CO)_6]_3^{2-}$ in NaY (1.3 nm). Each Pt cluster anion is formed successively by the following reductive carbonylation using a templating micro/mesoporous confined space of FSM-16 (2.8 and 4.7 nm), similarly in the solution [13–17,32,33],

$$H_2PtCl_6 + 3CO + H_2O \rightarrow \left[Pt(CO)Cl_3\right]^- \quad \text{in FSM-16 (4.7 nm)}$$

$$\rightarrow \textit{cis}\text{-}Pt(CO)_2Cl_2 + CO_2 + 4HCl \quad \text{in FSM-16 (2.8 nm)}$$

$$3n\,\textit{cis}\text{-}Pt(CO)_2Cl_2\left(\left[Pt(CO)Cl_3\right]^-\right) + (3n+1)H_2O + 6n\,HCl + (3n+1)CO_2 \rightarrow H_2\left[Pt_3(CO)_6\right]_n + 3n\,HCl + (3n+1)CO_2$$

where n is valuable from 5 and 6 in FSM-16 (2.8 nm and 4.7 nm), respectively.

In the first stage of the cluster formation, a preabsorbed water in NaY and FSM-16

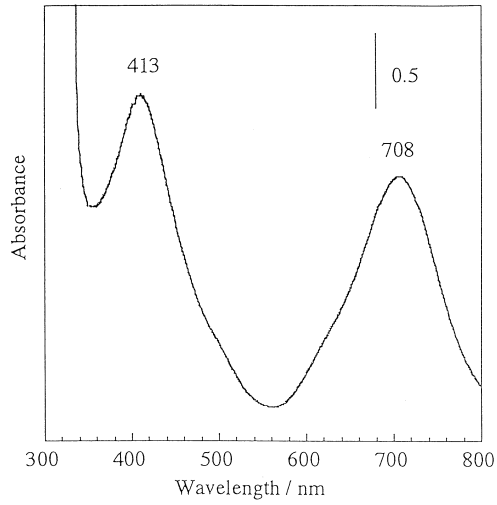

Fig. 3. UV–Vis spectra of Pt carbonyl cluster anions extracted with $(Ph_3P)_2NCl$ in THF from the sample of H_2PtCl_6/NEt_4Cl/FSM-16 (4.7 nm) after the reductive carbonylation at 323 K.

was consumed with CO to reduce Pt^{2+}/NaY, $Pt(NH_3)_4^{2+}$/NaY and H_2PtCl_6/FSM-16 to form *cis*-$Pt(CO)_2Cl_2$ and $Pt(CO)Cl_3$. It is interesting to find that the deferent carbonyl species such as $[Pt(CO)Cl_3]^-$ in FSM-16 (4.7 nm) and *cis*-$Pt(CO)_2Cl_2$ in FSM-16 (2.8 nm) are formed as the intermediate for the Chini Pt cluster anions. As shown in Fig. 1, it is suggested that an excess amount of water promotes a further clustering of the Pt carbonyls due to the water gas shift reaction. As the analogy of 'ship-in-bottle' synthesis of $[Pt_3(CO)_6]_n^{2-}$ ($n = 3,4$) in NaY [14,15], the successive oligomerization of *cis*-$Pt(CO)_2Cl_2$ to form $[Pt_3(CO)_6]_5^{2-}$ in FSM-16 (2.8 nm) and $[Pt_3(CO)_6]_6^{2-}$ in FSM-16 (4.7 nm) possibly via an intermediate triangular cluster '$Pt_3(CO)_6$' (2100s, 1896m and 1841m cm^{-1}) [14,15] in the channels of FSM-16. Calabrese et al. [29] and Longoni and Chini [30] have reported that the trigonal prismatic Pt frameworks are elongated in the acidic/oxidative circumstance, whereas they are shorten in the basic/reductive one. The results suggest that the channel-wall of FSM-16 (4.7 nm) having a weaker basicity prefers to synthesize a larger Pt cluster anion (8 Å × 15 Å) via a $[Pt(CO)Cl_3]^-$ which is accommodated in its mesoporous channel of FSM-16 (4.7 nm), compared with that of FSM-16 (2.8 nm), as pictorially represented in Fig. 4.

3.3. Confinement of Pt carbonyl cluster anions in the mesoporous channels of FSM-16

The CO bands of the Chini-type Pt carbonyl clusters are affected by the supporting materials such as SiO_2, Al_2O_3 and MgO, as summarized in Table 1. In particular, it is interesting to note that the CO bands of the confined Pt cluster anions $[Pt_3(CO)_6]_n^{2-}$ ($n = 3$ and 4) in the micropores of NaY (1.3 nm) are substantially shifted to higher frequencies ($\Delta\nu(CO) = 15$–25 cm^{-1}) for linear CO and lower ($\Delta\nu(CO) = -35$–45 cm^{-1}) for bridging one, as presented in Table 1. The CO band shifts are originated in conjunction with the interaction of Pt cluster anions and acid/base sites on supporting materials [40]. For a robust Pt cluster anion such as $[Pt_3(CO)_6]_5^{2-}$ in a mesoporous channel of FSM-16 (2.8 nm), both bands of the linear and bridging CO shifts to higher frequency ($\Delta\nu(CO) = 30$ and 25 cm^{-1}), similar to the cluster anion impregnated on silica surface. Such a CO band shift may be owing to the proton interaction between the cluster anion and silanol (Si–OH) and acidic sites such as Al^{3+} on the internal wall of FSM-16 (Si/Al = 320). By contrast with FSM-16 (2.8 nm) as a host, there are not appreciable frequency shifts of both CO bands ($\Delta\nu(CO) = 3$ and 5 cm^{-1}) for $[Pt_3(CO)_6]_6^{2-}$ formed in FSM-16 having a lager channel of 4.7 nm. This implies that the Pt cluster anions are free from any cluster confinement similarly in the THF and MeOH solution. This is caused by a weaker interaction of Pt_{18} anion with the acidic wall of a wider channel of FSM-16 (4.7 nm) in comparison with the cluster anion in FSM-16 (2.8 nm). Moreover, it is interesting to find that the exposure of the solid sample $[Pt_3(CO)_6]_5^{2-}$ in FSM-16 (2.7 nm) to THF vapor resulted in a marked change of color from reddish-brown to dark-green ($\lambda_{max} = 290$w, 409m and 698s nm, which resembles that of $[Pt_3(CO)_6]_5^{2-}$ in MeOH solution ($\lambda_{max} = 271$w, 408m and 697s nm). It is proposed to explain the different reflectance UV–Vis spectrum of the dried sample of Pt cluster anions in FSM-16 (2.8 nm) from that of the solvated Pt cluster anion in solution might be owing to a cluster-assembling and cluster–support interaction in the confined channel space of FSM-16 (2.8 nm), compared with FSM-16 (4.7 nm).

3.4. Cluster-derived Pt nanoparticles in FSM-16

According to the previous work by the in situ FTIR and EXAFS observation [32,33], it was demonstrated that the Pt cluster anions in FSM-16 such as $[Pt_{15}(CO)_{30}]^{2-}/Et_4NCl$/FSM-16 (2.8 nm) (2075s and 1875m cm^{-1}) were gradually transformed by evacuation by heating at 300–343 K, resulting in a partially decarbony-

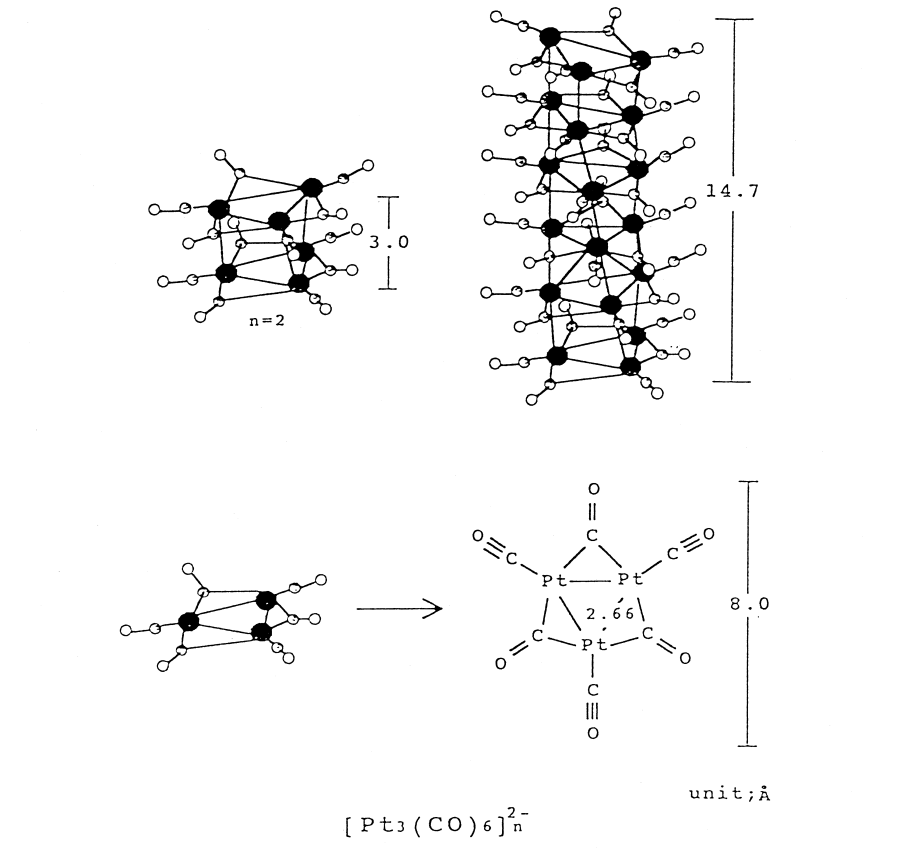

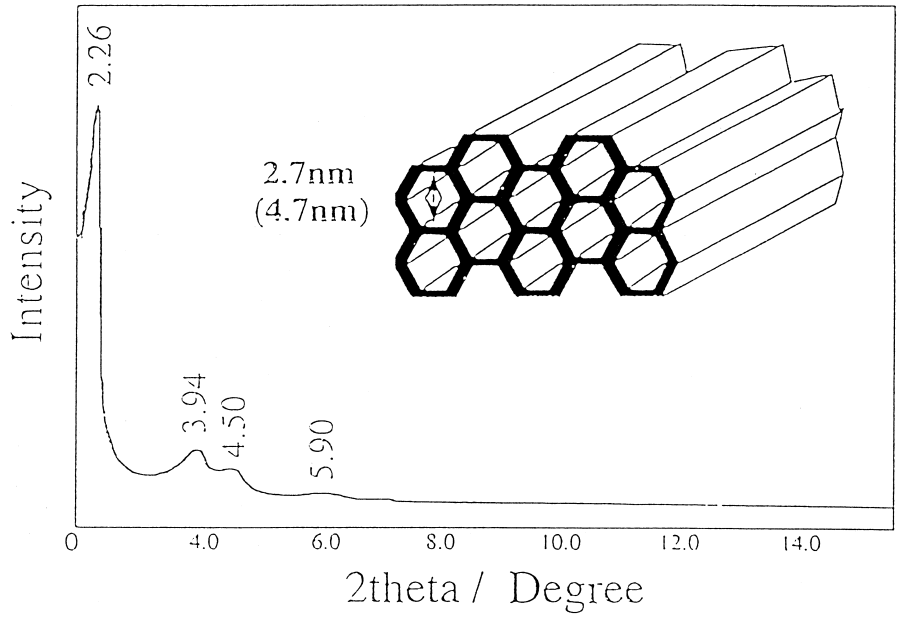

Fig. 4. Pictorial representation of Chini-type Pt carbonyl cluster anions $[Pt_3(CO)_6]_n^{2-}$ ($n = 6$) guest and mesoporous material FSM-16 host having a hexagonal ordered channels of 2.8 and 4.7 nm. (characterized by the XRD pattern).

lated cluster owing to the successive removal of CO. Fig. 5 represents the change of IR spectra of $[Pt_3(CO)_6]_6^{2-}/NEt_4Cl/FSM\text{-}16$ (4.7 nm) by heating at 300–523 K to 1×10^{-3} kPa. When the sample was evacuated at 323 K, the bridging CO band preferentially decreased and eventually disappeared, compared with those of terminal CO. The linear CO band was relatively enhanced in its intensity and subsequently decreased and broadened above 323 K. In addition, the peak position of linear CO shifted to lower frequencies from 2056 to 2010 cm^{-1} by the prolonged thermal evacuation, as shown in Fig. 5c–g. By heating the sample above 473 K, the terminal CO eventually disappeared (Fig. 5h–i). The results suggest that the bridging CO of $[Pt_3(CO)_6]_6^{2-}$ in FSM-16 (4.7 nm), similar to $[Pt_3(CO)_6]_5^{2-}$ in FSM-16 (2.8 nm) [32,46] was partially switched to the linear one by the controlled thermal evacuation at 300–323 K. This

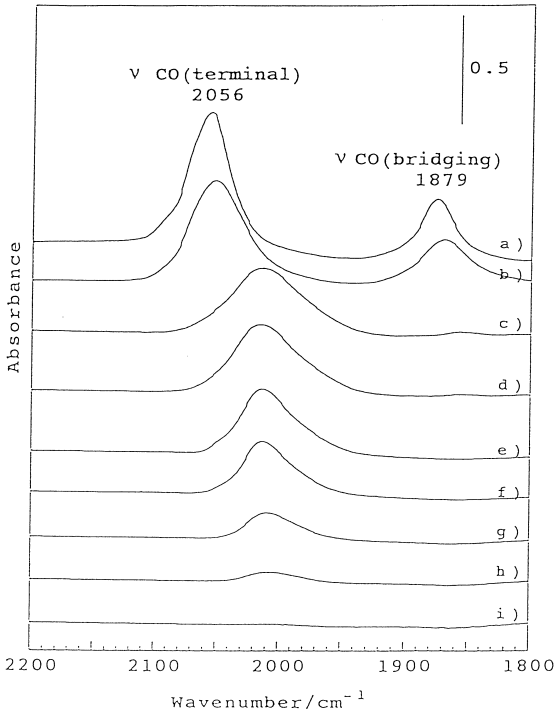

Fig. 5. IR spectra of $[Pt_3(CO)_6]_6^{2-}/NEt_4Cl/FSM\text{-}16$ (4.7 nm) after the thermal evacuation for 1 h at various temperatures. (a) 300 K, (b) 323 K, (c) 343 K, (d) 373 K, (e) 423 K, (f) 473 K, (g) 493 K, (h) 523 K, and (i) 623 K, respectively.

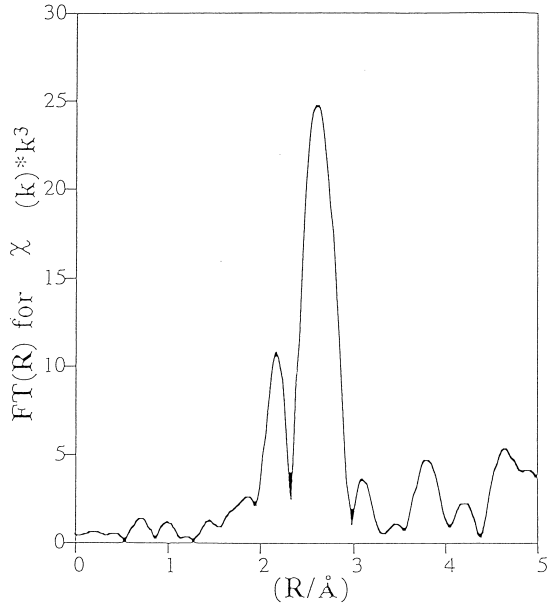

Fig. 6. Fourier transforms of k^3 weighted EXAFS of $[Pt_3(CO)_6]_6^{2-}/NEt_4Cl/FSM\text{-}16$ (4.7 nm) after evacuated at 473 K for 2 h in the k range of 3.5–18 $Å^{-1}$.

was followed with an exceeding removal of the linear and bridging CO at 473 K. Both CO bands characteristic of $[Pt_3(CO)_6]_5^{2-}$ in FSM-16 were not regenerated by the admission of CO upon the sample decarbonylated above 323 K, implying that an irreversible transformation of the Pt carbonyl cluster proceeds to cluster agglomerization by the thermal evacuation. Fig. 6 shows the Fourier transforms of k^3 weighted EXAFS of $[Pt_3(CO)_6]_6^{2-}/NEt_4Cl/FSM\text{-}16$ (4.7 nm) after the sample was evacuated at 473 K for 2 h. Table 2 shows the EXAFS parameters, e.g., the C.N. and interatomic distance R for Pt–Pt of the sample after the thermal treatments at 473 K in a vacuum. The resulting Fourier Transform pattern (Fig. 6) consists of a single Pt–Pt peak, which is characteristic of spherical Pt particles. The EXAFS results (C.N. = 7.9, $R = 2.74$ Å for Pt–Pt) suggest that two or three cluster molecules of a cylindrical $[Pt_3(CO)_6]_6^{2-}$ come together and transform to a nanometer size Pt particle of 1.5 nm consisting of 40–50 Pt atoms. This sample is referred to as

Table 2
Structural EXAFS parameters for the samples of Pt nanowires prepared in FSM-16 having 2.8 and 4.7 nm channel size by photoreduction of H_2PtCl_6/FSM-16 under 2-propanol and water at 300 K, compared with those for the samples of Pt nanowires/FSM-16

Sample	Bond	R (Å)	C.N.	E (eV)	σ^2 (Å^2)	R factor
(a) Pt nanowire/FSM-16 (2.8 nm) 5% wt. Pt loading mass	Pt–Pt	2.74	7.8	−1.6	7.7×10^{-3}	9.8
(b) Pt nanowire/FSM-16 (4.7 nm) 5% Pt loading mass	Pt–Pt	2.75	8.9	3.8	4.7×10^{-3}	3.0
(c) Pt nanowire/FSM-16 (4.7 nm) 10% Pt loading mass	Pt–Pt	2.74	9.4	−1.7	7.1×10^{-3}	9.4
(d) Pt nanoparticle/FSM-16 (2.8 nm) 5% Pt loading mass	Pt–Pt	2.72	6.7	1.2	3.4×10^{-4}	0.1
(e) Pt nanoparticle/FSM-16 (4.7 nm) 5% Pt loading mass	Pt–Pt	2.74	7.9	−1.8	7.4×10^{-4}	0.2

R (Å): interatomic distance for Pt–Pt.
C.N.: coordination number for Pt–Pt bond.

Pt nanoparticle/FSM-16 (4.7 nm). The EXAFS parameters (C.N. of Pt–Pt is 7.9 and those of Pt–C and Pt–O being less than 0.1) imply that all the surface Pt atoms of the particle in FSM-16 are naked, and the ratio of surface/bulk Pt atom is 0.45. The dispersion of Pt particles in FSM-16 (4.7 nm) was estimated by CO chemisorption, showing the CO chemisorption stoichiometry (CO/Pt) of 0.43. From the EXAFS and IR data in Figs. 5 and 6 and Table 2 suggest that the Pt_{18} carbonyl clusters in the channels of FSM-16 were subsequently transformed to the Pt nanoparticles of 1.5 nm, which is relatively larger than those (C.N.(Pt–Pt) = 6.7, $R = 2.72$ Å; average particle size = 1.2 nm) which are derived by a similar procedure from $[Pt_3(CO)_6]_5^{2-}$/NEt_4Cl/FSM-16 (2.8 nm) [46]. TEM picture of the sample of Pt cluster anions in FSM-16 (4.7 nm) after heating at 473 K for 2 h consists of small Pt particles of 2.0–3.0 nm diameter which were uniformly scattered and aligned in the mesoporous channels of FSM-16 (4.7 nm). The average size (2–3 nm) of Pt particles in FSM-16 (4.7 nm) by the TEM observation is relatively larger than the value of 1.5 nm estimated from the EXAFS results (in terms of the C.N. = 7.9). This is reasonably explained by the distortion of the Pt nanoparticles owing to the metal–oxygen interaction at the wall of FSM-16 channels. According to the EXAFS, FTIR, TPD and TEM studies, it was demonstrated that $[Pt_3(CO)_6]_6^{2-}$ encapsulated in the channels of FSM-16 (4.7 nm), similar to $[Pt_3(CO)_6]_5^{2-}$ in FSM-16 (2.8 nm) [32,46] are transformed by a controlled pyrolysis towards Pt nanoparticles as depicted in Scheme 1, owing to the controlled removal of CO by the thermal evacuation at 300–473 K.

3.5. Templating fabrication of Pt nanowires using the mesoporous channels of FSM-16 by the exposure to γ-ray and UV-irradiation

A sample of H_2PtCl_6/FSM-16 containing 3–10 mass% Pt was exposed to ^{60}Co γ-ray (adsorbed dose disintegration of 5000 Ci) at 300 K under the atmosphere of 2-propanol (15.0 kPa) and water (2.0 kPa) by (adsorbed dose disintegration of 5000 Ci). The color of the powdered sample of H_2PtCl_6/FSM-16 in a quartz-cell changed from pale yellow to gray by the exposure of γ-ray for 5–15 h. Fig. 7a represents an electron micrograph of H_2PtCl_6/FSM-16(2.8 nm diameter; 5 wt.% Pt loading) after the exposure of ^{60}Co γ-ray for 24 h at 300 K, showing the nanostructured Pt wires of 3 nm diameter which are scattered and aligned with the mesoporous channels of FSM-16. The diameter of the Pt wires is coincided to that of

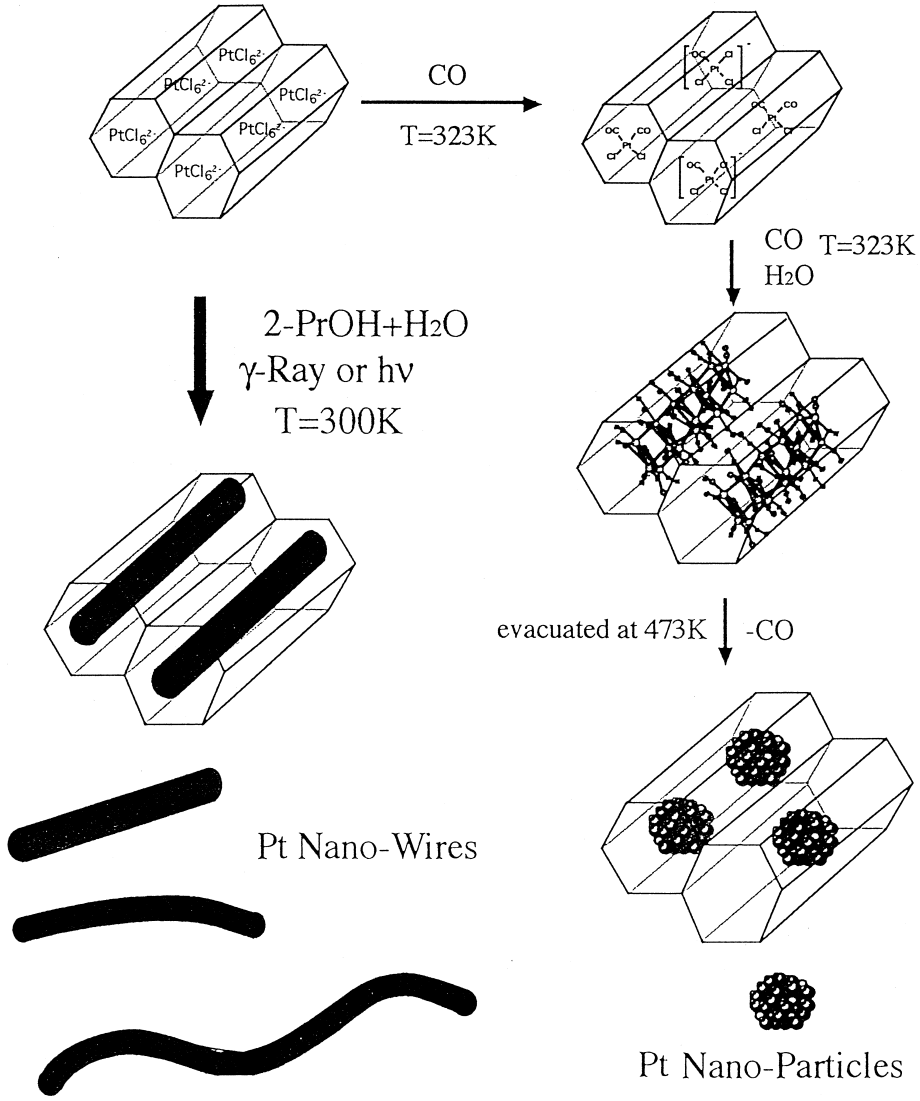

Scheme 1. Proposed templating fabrication of Pt nanoparticles derived from the Chini Pt cluster anions $[Pt_3(CO)_6]_n^{2-}$ ($n = 5, 6$) synthesized in mesoporous channels of FSM-16 by the controlled removal of CO, and Pt nanowires by the exposure of H_2PtCl_6/FSM-16 with 2-propanol and water to γ-ray or UV-light illumination.

cylindrical mesopores of the used FSM-16 (2.8 nm). It was interesting to find that the Pt nanowires consist of not only a cylindrical rod, but also some twisted and bent ones. Possibility of the twisting and bent Pt wires formed in FSM-16 is well- reflected in the existence of a disordered channel of FSM-16, as previously reported by Ryoo [47,48]. In addition, it was interesting to find that a high resolution electron micrograph of a single Pt wire (twisted) in FSM-16 as shown in Fig. 7b shows a clear pattern of the uniform lattice fringes ($d = 2.27$ Å), which are parallel to (110) plane of cubic symmetry. This implies that a Pt wire consists of a single crystal of (110) cubic symmetry, but not a linear chain (or ensemble) of the individual Pt particles. The TEM observation of the Pt nanowire in FSM-16 shows that the length of Pt nanowires is distributed in the dimension of 50–500 nm.

On the other hand, using the host FSM-16 having the larger channels of 4.7 nm, a similar ^{60}Co γ-ray irradiation of H_2PtCl_6/FSM-16 (4.7 nm) for 24 h at 300 K under the vapor of 2-propanol and water yielded the cylindrical Pt nanowires (4 nm diameter), which are densely aligned in the mesoporous channels of FSM-16 (4.7 nm). The length of the nanowire extends to 200–500 nm in FSM-16 (2.8 and 4.7 nm). The results suggest that the cylindrical channels of FSM-16 of 2.8 and 4.7 nm play a role as a templating host to prepare the Pt nanowires by the photoreduction of Pt species with the reductant reagent such as 2-propanol.

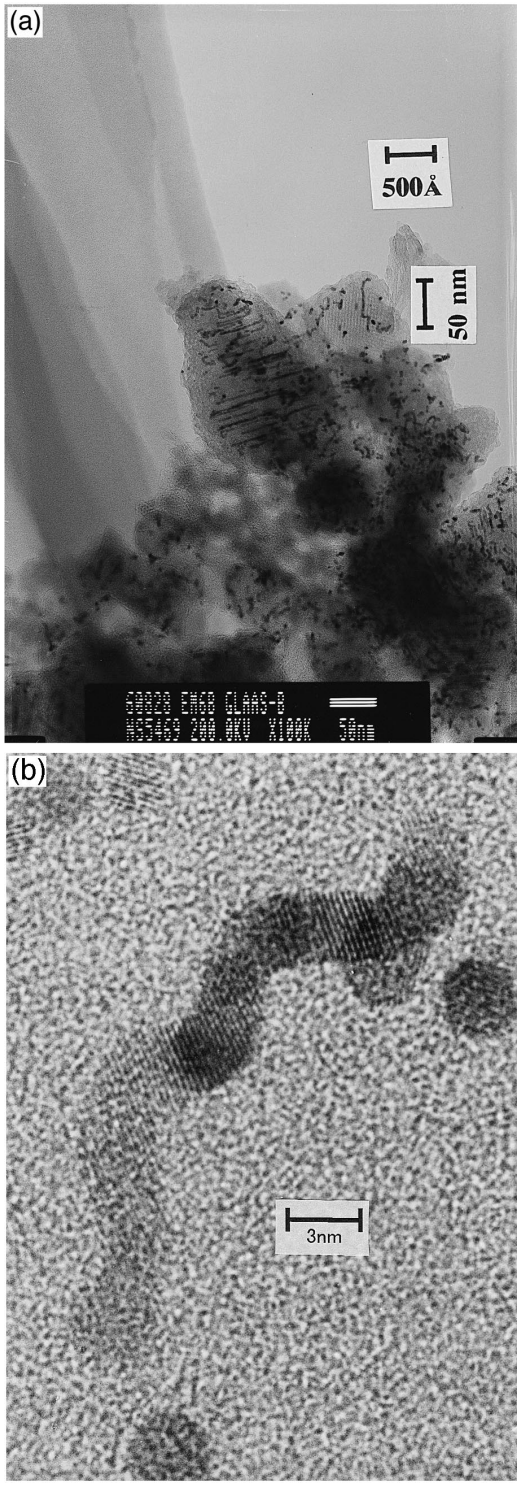

Fig. 7. Transmission electron microgram of (a) Pt-wire/FSM-16 (2.8 nm) prepared by reduction of H_2PtCl_6/FSM-16 with propanol + water under the γ-ray irradiation at 300 K for 5 h. The nanostructured wires (4 nm size × 50–100 nm long) were aligned in the ordered channels of FSM-16 (2.8 nm). (b) a close view of a single strain of Pt wire in FSM-16 (2.8 nm) which shows a clear diffraction image characteristic of (110) *bcc* lattice fringe; d = 2.256 Å.

A similar sample of the Pt nanowires in FSM-16 was prepared at 300 K by the exposure of H_2PtCl_6/FSM-16 (2.8 nm) charged in a quartz cell to the UV-light with a high pressure Hg lamp ($\lambda > 254$ nm) under the vapor of 2-propanol (35 kPa) and water (2.0 kPa). Fig. 8a showed that the photoreducing sample of the Pt nanowires of 2.8 nm diameter and 200–500 nm length, similar to those by the exposure of ^{60}Co γ-ray (Fig. 7). As shown in Fig. 8a, the Pt nanowires are scattered and rather uniformly formed in alignment with the ordered mesoporous channels of FSM-16, indicating that the wire formation proceeds through over the supports of FSM-16. Moreover, it was found that the lengths of Pt nanowires formed in FSM-16 are widely distributed from 100 to 500 nm for the sample of 5 wt.% loading Pt nanowire/FSM-16 (2.8 nm) by the exposure of the UV-light for 5 h, as shown in Fig. 8b. It was suggested from some additional experiments that the average lengths of the Pt nanowires in FSM-16 are proportionally increased from 50 to 500 nm by varying the loading of Pt(3–10 wt.%) and time exposure of ^{60}Co γ-ray and UV-light (4–20 h).

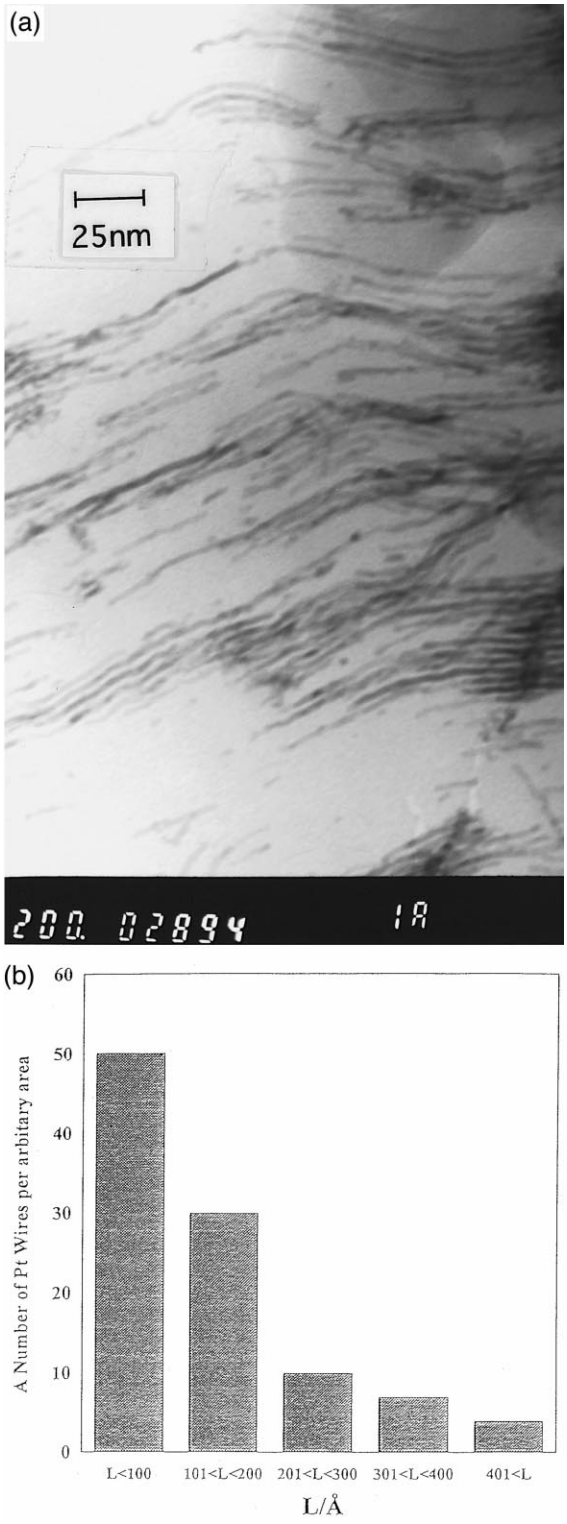

Fig. 8. Transmission electron microgram of (a) Pt nanowire/FSM-16 (2.8 nm) which were prepared by the exposure of 10 wt.% Pt mass loading H_2PtCl_6/FSM-16 (2.8 nm) with 2-propanol/water to the UV-irradiation at 300 K (using a high-pressure Hg lamp for 5 h), respectively. The cylindrical Pt nanowires (3 nm size×250–500 nm long) were extended and aligned in the ordered channels of FSM-16 (2.8 nm). (b) The distribution of lengths in the Pt nanowires formed from the 5% Pt mass loading H_2PtCl_6/FSM-16 (2.8 nm) by the exposure to the UV-light for 5 h. The cylindrical Pt nanowires (3 nm size×100–500 nm long) were extended and aligned in the ordered channels of FSM-16 (2.8 nm).

In order to investigate the structural property of the Pt nanowires in FSM-16, some XAFS measurements of the Pt-L_{III} edge (11562 eV) were carried out in the transmission mode. Fig. 9 represents the Pt-L_{III} edge XANES function of the sample of Pt nanowires in FSM-16 (2.8 nm), which was prepared by the exposure of 5 wt.% mass loading H_2PtCl_6/FSM-16 (2.8 nm) with 2-propanol (35 kPa) and water (2.0 kPa) to the UV-light using a high pressure Hg lamp at 300 K for 5 h. It is of interest to find that the X-ray absorption near edge spectrum (XANES) of the Pt nanowires/FSM-16 resembles those of the Pt cluster anions in FSM-16 (2.8 nm) and Pt foil, rather than that of the Pt nanoparticle in FSM-16.

The EXAFS parameters for the sample of Pt wires/FSM-16 (2.8 nm) by exposure of UV-light were evaluated by Fourier transform curve-fitting analysis, giving an average Pt–Pt C.N. = 7.8 and Pt–Pt interatomic distance R = 2.74 Å and a negligible contribution of Pt–O bond. As shown in Table 3, the samples for Pt nanowires/FSM-16 (4.7 nm) show the EXAFS parameters of C.N.(Pt–Pt) increasing from 8.9 to 9.8, possibly due to not only the increase of the wire-size, but also the average elongation of Pt nanowires from 100 to 500 nm, The mechanism for the templating fabrication of Pt nanowires in the FSM-16 channels by the exposure of γ-ray and UV-light has not been understood, but it is plausible that H_2PtCl_6/FSM-16 impregnated in FSM-16 is successively reduced by the exposure of ^{60}Co γ-ray and UV-light in

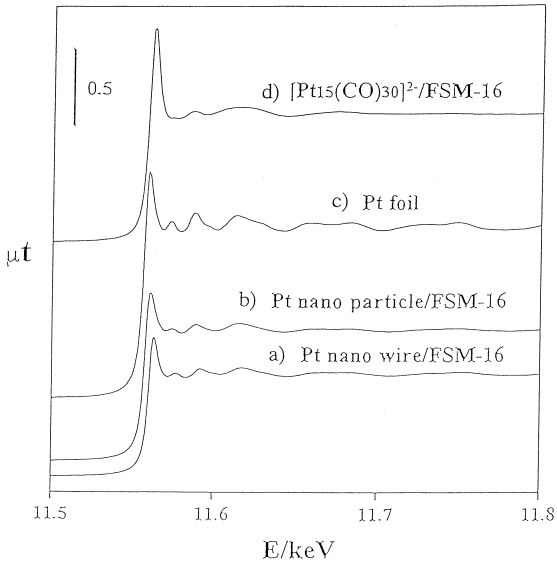

Fig. 9. Pt L(III) edge XAFS spectra for (a) the Pt nanowires/FSM-16 (2.8 nm) sample prepared by the templating reduction of H_2PtCl_6/FSM-16 (5 wt.% Pt loading) with propanol + water under the UV-light irradiation at 300 K for 5 h, compared with those of (b) Pt nanoparticle/FSM-16 (2.8 nm), (c) Pt foil, and (d) $[Pt_3(CO)_6]_6^{2-}/NEt_4Cl$/FSM-16 (2.8 nm).

the presence of 2-propanol and water, which yields highly active reductant species such as a solvated electron, H atom and a $(CH_3)_2COH$ radical, as previously proposed for Pt particles in solution by the radiolytic reduction [49]. It is conceivable that produced Pt atoms are oligomerized to rod-like ensembles, extending to Pt nanowires which are templated by a cylindrical channels of FSM-16 having the different open-ends of 2.8 and 4.7 nm.

3.6. Chemisorption of CO and H_2 on the Pt nanowires / FSM-16

The IR observation was conducted on CO chemisorption at 300 K for the sample of the Pt nanowire/FSM-16 (2.8 nm) after the sample was reduced with hydrogen at 523 K for 1 h and evacuated at 523 K for 0.5 h. A weak and broad band appeared at 2080 cm^{-1} which is assignable to a linear CO. This resembles a linear CO attached (2085 cm^{-1}) on a single crystal Pt(111) and (110) surface [43], although shifted to a lower frequency. By contrast, the samples of Pt nanoparticles (1.1 nm)/FSM-16 (2.8 nm) yielded the linear CO bands at 2060 cm^{-1}, having over 10 times larger intensity with a medium band of the bridging one (1845 cm^{-1}), compared with those of the sample of Pt nanowires in FSM-16, as shown in Fig. 10. In fact, the amounts of CO and H_2 chemisorption on the Pt nanowires in FSM-16 were measured as one-order magnitude smaller than those on the samples of Pt-nanoparticle in FSM-16. The results for the adsorption isotherms of CO and H_2 demonstrated that the adsorption stoichiometries (dispersion parameter; CO/Pt and H/Pt) on the samples of Pt nanowire/FSM-16 (2.8 nm) are 0.03 and 0.04 at 300 K, respectively, in comparison with those (CO/Pt = 0.45 and H/Pt = 0.40) for the samples of Pt nanoparticle/FSM-16 (2.8 nm). The differences in chemisorption of CO and H_2 is implicated in those of the surface Pt atoms available for the Pt

Table 3
Catalytic performances in water gas-shift reaction (WGSR) on $[Pt_{15}(CO)_{30}]^{2-}$, Pt nanowires and Pt nanoparticles in FSM-16 (2.8 nm), compared with those on $[Pt_3(CO)_6]_n^{2-}$ ($n = 3, 4$)/NaY and Pt/γ-Al_2O_3

Pt carbonyl clusters/ FSM-16 or NaY	WGSR ($CO + H_2O \rightarrow CO_2 + H_2$)	
	k/min (323 K)[a]	Activation energy (kJ/mol)
$[Pt_{15}(CO)_{30}]^{2-}[NEt_4]_2^+$/ FSM-16 (2.8 nm)	60	28
$[Pt_{15}(CO)_{30}]^{2-}[NBu_4]_2^+$/ FSM-16 (2.8 nm)	23	–
$[Pt_{12}(CO)_{24}]^{2-}$/ NaY (1.3 nm)	2.1	–
$[Pt_9(CO)_{18}]^{2-}$/ NaY (1.3 nm)	3.8	40
Pt nanowire/ FSM-16 (2.8 nm)	110	20
Pt nanoparticle/ FSM-16 (2.8 nm)	1.3	48
Pt/γ-Al_2O_3[b]	0.1	–

[a] CO (200 Torr) + H_2O (15 Torr); TOF(CO_2) (mmol/Pt atom/min): Pt surface is estimated by CO chemisorption.
[b] The catalyst was prepared by H_2-reduction at 673 K for 2 h after H_2PtCl_6 impregnated on γ-Al_2O_3 (4 mass% Pt).

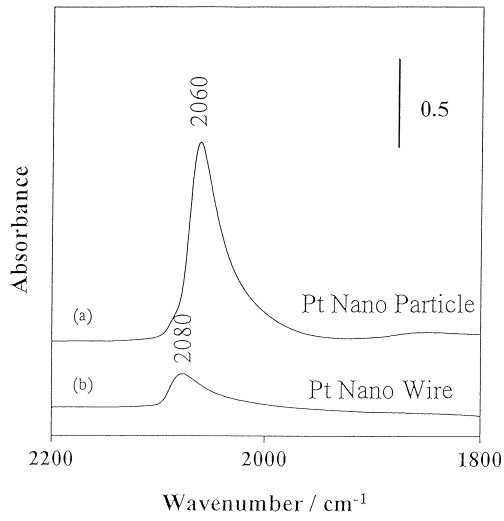

Fig. 10. IR spectra for CO chemisorption on the samples of Pt nanoparticles/FSM-16 (2.8 nm) and Pt nanowire/FSM-16 (2.8 nm). The samples were applied to hydrogen reduction at 423 K for 1 h, followed with the evacuation at 423 K for 0.5 h, prior to the IR measurement.

nanowires and particles in FSM-16. The Pt nanowires are strictly confined with the channel walls of FSM-16, while the most surface Pt atoms of nanoparticles in FSM-16 are available for the adsorption of CO and H_2.

3.7. Catalytic performances for WGSR on Pt cluster anions, Pt nanoparticles and nanowires in FSM-16

To investigate the catalytic performances of the Pt carbonyl cluster anions, Pt nanowire and Pt nanoparticles encapsulated in FSM-16 concerning their structural confinement and cluster–support interaction, we study the specific activation of CO and water in the water gas shift reaction (WGSR) under the mild reaction conditions. The reaction ($CO + H_2O \rightarrow CO_2 + H_2$) was performed at 300–393 K to a reduced pressure ($p_{CO} = 5$–27.5 kPa and $p_{H_2O} = 1.5$–2.6 kPa) by using a closed circulating Pyrex glass reactor charged with the powdered samples of $[Pt_{15}(CO)_{30}]/[NEt_4]_2$/FSM-16, Pt nano particle/FSM-16 (2.8 nm), Pt nanowire/FSM-16 (2.8 nm) including $[Pt_{12}(CO)_{24}]^{2-}$/NaY and $[Pt_9(CO)_{18}]^{2-}$/NaY as confined metal clusters in a microporous space. The samples of the Pt nanowire/FSM-16 and Pt nanoparticle/FSM-16 were applied to the hydrogen reduction at 523 K for 2 h prior to the WGSR. As shown in Table 3, $[Pt_{15}(CO)_{30}]^{2-}$ cluster anions [32,33] and Pt nanowires in FSM-16 exhibited remarkably high activities in the WGS reaction to form an equimolar mixture of CO_2 and H_2, compared with the Pt_{12}–Pt_9 cluster in NaY [14,15] and Pt nanoparticle in FSM-16 even the conventional Pt/Al_2O_3 catalyst (4 mass% Pt). It was worthy to note that the turnover rates (TOF; mmol(CO_2)/Pt surface atom/min) for the WGSR at 323 K on the sample of Pt nanowires in FSM-16 (2.8 nm) are higher by 60–90 times magnitude than those on the Pt nanoparticles in FSM-16 (2.8 nm). The turnover rates of WGS reaction at 323 K on $[Pt_{15}(CO)_{30}]^{2-}$ in FSM-16 are comparable with those on the Pt nanowires in FSM-16, which are higher (20–100 times) than those on Pt nanoparticles in FSM-16 and $[Pt_{12}(CO)_{24}]^{2-}$ and $[Pt_9(CO)_{18}]^{2-}$ (4 mass% Pt) entrapped in NaY cavities. Moreover, it was demonstrated that the activation energies for the WGSR are smaller (28–32 kJ/mol) on $[Pt_{15}(CO)_{30}]^{2-}$ and Pt nanowires in FSM-16 in comparison with those (45–52 kJ/mol) on those on Pt nanoparticles in FSM-16 and $[Pt_{12}(CO)_{24}]^{2-}$ and $[Pt_9(CO)_{18}]^{2-}$ (4 mass% Pt) entrapped in NaY cavities. From these evidences, it is suggested that the surface Pt atoms exposed to the nanowires are extremely active for the WGSR, compared those to the nanoparticles entrapped in the confined channels of FSM-16 (2.8 nm). The unusually higher turnover-rates of the Pt nanowires in FSM-16 for WGSR are implicated in the anisotoropic morphological differences of the Pt nanowires in comparison with the nanoparticles, possibly owing to the larger interaction (or larger contact) of the Pt wires with the channel surface of FSM-16, which is negatively charged. It is conceivable that the adsorbed water is favorable to be polarized on the negatively charged surface Pt atoms of the nanowires in FSM-16, which promote the

WGSR, similar to the Pt cluster anions in FSM-16. They exhibit higher activities in the WGSR probably owing to their flexible cluster frameworks and sufficient diffusibility of reactant gases in the mesoporous channels of FSM-16 (2.8 and 4.7 nm), compared with the Pt_9 and Pt_{12} carbonyl clusters which are restricted in NaY micropore constrain (1.2 nm diameter).

4. Conclusion

(1) The Chini-type Pt carbonyl cluster anions such as $[Pt_3(CO)_6]_6^{2-}$ are synthesized via $[Pt(CO)Cl_3]^-$ in a larger channel of FSM-16 (4.7 nm) by the reductive carbonylation of H_2PtCl_6 at 323 K, similar to $[Pt_3(CO)_6]_5^{2-}$ via *cis*-$Pt(CO)_2Cl_2$ which is formed in that of FSM-16 (2.8 nm).

The extracted Pt cluster anions with [PPN]Cl by the cation metathesis is identified as $[Pt_3(CO)_6]_6^{2-}$ in FSM-16 (4.7 nm) by FTIR and UV–Vis spectroscopy.

(2) The EXAFS, TEM and FTIR studies suggest that $[Pt_3(CO)_6]_6^{2-}$ anions in FSM-16 (4.7 nm) are transformed by the controlled removal of CO to the partially decarbonylated Pt clusters, and eventually converted into Pt nanoparticles of 1.5 nm size by heating above 473 K, as indicated in Scheme 1.

(3) The platinum nanowires [3–4 nm (diameter) × 50–500 nm (long)] are prepared using the cylindrical mesoporous hosts of FSM-16 (2.8 and 4.7 nm) in a templating reduction of H_2PtCl_6/FSM-16 by the exposure to ^{60}Co γ-ray or UV-light ($\lambda_{max} > 254$ nm) under the atmosphere of 2-propanol and water (Scheme 1).

(4) The Pt nanowires in FSM-16 (2.8 and 4.7 nm) showed a very weak IR band assignable to the linear CO chemisorption owing to the strict confinement with the channel wall of FSM-16, but exhibited the remarkable activities per surface Pt atoms (TOF) for a water gas-shift reaction at 323–393 K by 60–90 times magnitude larger than those of Pt nanoparticles in FSM-16.

Acknowledgements

This work was supported by Grant-Aid (09232204) through Ministry of Education, Science, Sports and Cultures, Japan. The EXAFS experiments were performed at National Laboratory of High Energy Physics, Synchroton Radiation Beam Line. The authors thank Dr. S. Inagaki and Dr. Y. Fukushima of Toyota Central Laboratory for providing the mesoporous materials of FSM-16 (2.8 and 4.7 nm), and their helpful discussion on the TEM characterization of the samples of the Pt particles and Pt nanowires in FSM-16.

References

[1] M. Ichikawa, Adv. Catal. 38 (1992) 283.
[2] T. Maschmeyer, F. Rey, G. Sankar, J.M. Thomas, Nature 378 (1995) 159.
[3] G.A. Ozin, S. Ozkar, Chem. Mater. 4 (1992) 511.
[4] R. Leonm, D. Margolese, G. Stucky, P.M. Petroff, Phys. Rev. B 52 (1995) 2285.
[5] M. Ichikawa, Polyhedron 7 (1988) 2351.
[6] A. Fukuoka, T. Kimura, L.-F. Rao, N. Kosugi, H. Kuroda, M. Ichikawa, Catal. Today 6 (1988) 55.
[7] M. Ichikawa, Chemisorption and Reactivity on Supported clusters and thin films, in: R.M. Lambert, G.G. Pacchioni (Eds.), Kluwer Acad. Pub., 1997, pp. 153–192.
[8] L.-F. Rao, A. Fukuoka, N. Kosugi, H. Kuroda, M. Ichikawa, J. Phys. Chem. 94 (1990) 5317.
[9] M. Ichikawa, L.-F. Rao, T. Ito, A. Fukuoka, J. Chem. Soc. Faraday Disc. 87 (1988) 321.
[10] S. Kawi, B.C. Gates, J. Am. Chem. Soc. 115 (1993) 4830.
[11] S. Kawi, B.C. Gates, J. Chem. Soc. Chem. Commun., 1992, 702.
[12] A.-M. Liu, T. Shido, M. Ichikawa, J. Chem. Soc. Chem. Commun. (1995) 1337.
[13] A. De Mallmann, D. Barthomeuf, Catal. Lett. 5 (1990) 293.
[14] G.-J. Li, T. Fujimoto, A. Fukuoka, M. Ichikawa, J. Chem. Soc. Chem. Commun. (1991) 1337.
[15] G.-J. Li, T. Fujimoto, A. Fukuoka, M. Ichikawa, Catal. Lett. 12 (1992) 171.
[16] G. Schultz-Ekloff, R.J. Lipski, N.I. Jaeger, P. Hulstede, Catal. Lett. 30 (1995) 65.
[17] L. Kubelkova, L. Drozdova, L. Brabec, J. Novakova, J. Kotrla, G.S. Schultz-Ekloff, P. Hulstede, G. Schultz-Ekloff, J. Phys. Chem. 100 (1996) 15517.
[18] M. Ichikawa, A.M. Liu, G. Chen, T. Shido, Topics Catal. 2 (1995) 141.
[19] L.-F. Rao, T. Kimura, A. Fukuoka, M. Ichikawa, J. Chem. Soc. Chem. Commun. (1986) 458.
[20] A. Fukuoka, T. Kimura, L.-F. Rao, N. Kosugi, H. Kuroda, M. Ichikawa, Appl. Catal. 50 (1989) 295.

[21] M. Ichikawa, T. Kimura, A. Fukuoka, Stud. Surf. Sci. Catal. 60 (1991) 335.
[22] M. Ichikawa, T. Tanaka, W. Pan, R. Ohtani, R. Ohonishi, T. Shido, Stud. Surf. Sci. Catal. 69 (1996) 335.
[23] C.T. Kresge, M.E. Leonowicz, W.J. Roth, J.C. Vartuli, J.S. Beck, Nature 359 (1992) 710.
[24] J.S. Beck, J.C. Vartuli, W.J. Roth, M.E. Leonowicz, C.T. Kresge, K.D. Schmitt, C.T.-W. Chu, D.H. Olson, E.W. Sheppard, S.B. McCullen, J.B. Higgins, J.L. Schlenker, J. Am. Chem. Soc. 114 (1992) 10834.
[25] S. Inagaki, Y. Fukushima, K. Kuroda, J. Chem. Soc. Chem. Commun. (1993) 680.
[26] S. Inagaki, A. Koiwai, N. Suzuki, Y. Fukushima, K. Kuroda, Bull. Chem. Soc. Jpn. 69 (1996) 1449.
[27] C. Huber, K. Moller, T. Bein, J. Chem. Soc. Chem. Commun. (1994) 2619.
[28] M. Sasaki, M. Osada, N. Sugimoto, S. Inagaki, Y. Fukushima, A. Fukuoka, M. Ichikawa, Microporous Mesoporous Mater. 21 (1998) 597.
[29] J.C. Calabrese, L.F. Dahl, P. Chini, G. Longoni, S. Martinengo, J. Am. Chem. Soc. 96 (1974) 2614.
[30] G. Longoni, P. Chini, J. Am. Chem. Soc. 98 (1978) 7225.
[31] D.C. Chang, D.C. Koningberger, B.C. Gates, J. Am. Chem. Soc. 114 (1992) 6460.
[32] T. Yamamoto, T. Shido, S. Inagaki, Y. Fukushima, M. Ichikawa, J. Am. Chem. Soc. 118 (1996) 5810.
[33] M. Ichikawa, T. Yamamoto, W. Pan, T. Shido, Stud. Surf. Sci. Catal. 105 (1997) 679.
[34] User manual of Technos EXAFS analyzing program.
[35] D.C. Koningsberger, R. Prins, X-ray Adsorption: Principles, Applications, Techniques of EXAFS, SEXAFS, and XANES, Wiley, New York, 1988, p. 395.
[36] R.J. Irving, E.A. Magnussen, J. Chem. Soc. (1956) 1860.
[37] R.J. Irving, E.A. Magnussen, J. Chem. Soc. (1958) 2283.
[38] D.B. Dell'Amico, F. Calderazzo, C.A. Veracini, N. Zandona, Inorg. Chem. 23 (1984) 3030.
[39] J.N. Kondo, K. Yokota, K. Domen, C. Hirose, Catal. Lett. 40 (1996) 81.
[40] M. Ichikawa, Chem. Lett. (1976) 335.
[41] D.M. Mashecheck, M. Wucfrer, L.F. Dahl, A. Ceriotti, G. Longoni, M. Manassero, M. Sansoni, P. Chini, J. Am. Chem. Soc. 114 (1992) 6159.
[42] M.J. D'Aniaello Jr., C.J. Carr, M.G. Zammit, Inorg. Synthesis 26 (1989) 319.
[43] A. Crossley, D.A. King, Surf. Sci. 95 (1980) 131.
[44] J.D. Roth, G.J. Lewis, L.K. Safford, X. Jiang, L.F. Dahl, M.J. Weaver, J. Am. Chem. Soc. 114 (1992) 6159.
[45] T. Fujimoto, A. Fukuoka, S. Iijima, M. Ichikawa, J. Phys. Chem. 97 (1993) 279.
[46] T. Yamamoto, T. Shido, S. Inagaki, Y. Fukushima, M. Ichikawa, J. Phys. Chem. B 102 (1998) 3866.
[47] C.H.K., R. Ryoo, Chem. Commun. (1996) 2467.
[48] R. Ryoo, J.M. Kim, C.H. Ko, C.H. Shin, J. Phys. Chem. 100 (1996) 17718.
[49] A. Henglein, B.G. Ershov, M. Malow, J. Phys. Chem. 99 (1995) 14129.